

Additional complex conjugate feedback-induced explosive death and multistabilitiesK. Sathiyadevi ^{1,2} D. Premraj ³ Tanmoy Banerjee,⁴ and M. Lakshmanan⁵¹*Centre for Computation Biology, Chennai Institute of Technology, Chennai 600 069, Tamilnadu, India*²*Complex Systems and Applications Lab, Rajalakshmi Institute of Technology, Chennai 600124, Tamilnadu, India*³*Centre for Nonlinear Dynamics, Chennai Institute of Technology, Chennai 600 069, Tamil Nadu, India*⁴*Chaos and Complex Systems Research Laboratory, Department of Physics, University of Burdwan, Burdwan 713 104, West Bengal, India*⁵*Department of Nonlinear Dynamics, School of Physics, Bharathidasan University, Tiruchirappalli - 620 024, Tamil Nadu, India*

(Received 14 June 2022; accepted 15 August 2022; published 31 August 2022)

Many natural and man-made systems require suitable feedback to function properly. In this study, we aim to investigate the impact of additional complex conjugate feedback on globally coupled Stuart-Landau oscillators. We find that this additional feedback results in the onset of symmetry breaking clusters and out-of-phase clusters. Interestingly, we also find the existence of explosive amplitude death along with disparate multistable states. We characterize the first-order transition to explosive death through the amplitude order parameter and show that the transition from oscillatory to death state indeed shows a hysteresis nature. Further, we map the global dynamical transitions in the parametric spaces. In addition, to understand the existence of multistabilities and their transitions, we analyze the bifurcation scenarios of the reduced model and also explore their basin stability. Our study will shed light on the emergent dynamics in the presence of additional feedback.

DOI: [10.1103/PhysRevE.106.024215](https://doi.org/10.1103/PhysRevE.106.024215)**I. INTRODUCTION**

In many natural and man-made systems including neural networks, vision systems, lasers, etc., feedback is essential for proper functioning and it can be used for enhancing the performance of such systems [1–4]. Besides, several investigations have been conducted using various nonlinear models to get a better understanding of the dynamical characteristics as well as the impact of feedback [5–10]. Recent investigations reveal that appropriate feedback can restore oscillatory dynamics or induce the oscillation death state depending on the properties of the ensembles, coupling architecture, and the kind of feedback and its strength [11–13]. Importantly, among the various intrinsic and extrinsic parameters such as time delay, low-pass filtering, mean-field density, etc., typically, the feedback is used for controlling purposes [14–22]. For instance, the conjugate feedback or the self-feedback approach is used for controlling the birhythmicity in different realistic models such as energy harvesting systems as well as biochemical systems [23,24]. The self-feedback factor can also be used for controlling the spontaneous symmetry breaking oscillations [25]. The linear feedback in the diffusion term can cause suppression of aging whereas by providing the feedback in the mean-field term one can enhance the aging region [26–28]. The robustness of dynamical activity has also been demonstrated in damaged scale-free and small-world networks using external feedback mechanisms [29].

On the other hand, explosive transitions like explosive percolation (EP), explosive synchronization (ES), and explosive death (ED) have also been extensively studied in networks of coupled systems by various research groups [30–33]. Each of these transitions has its own merits and demerits. Among all

of them, explosive death is an interesting phenomenon that exhibits a first-order jump from oscillatory state to oscillation death state [34]. Understanding the reason behind the emergence of such ED may help to predict or prevent them earlier in real-time instances. Originally, the explosive death was reported in frequency weighted coupling under three different frequency distributions [34]. Subsequently, ED was also investigated in mean-field diffusive coupling, and the occurrence of ED was reported in van der Pol and Lorenz oscillators [35]. Later, it was also demonstrated in the coupled limit cycle and chaotic oscillators under different kinds of network topologies including nearest neighbors, all to all, nonlocal, and star network connectivities [36,37]. Very recently, conjugately coupled van der Pol oscillator induced ED (first-order transitions during the forward and backward transitions) and semi-ED (first-order transitions occur during forward transitions, while second-order transitions occur during backward transitions, or vice versa) have also been demonstrated [38]. Further, dynamical mean-field interaction induced ED was reported under the limit cycle, chaotic oscillators, and neural networks [39]. As of now, the explosive death state has been identified due to various kinds of interactions and frequency distribution. In this paper, *we examine whether an additional complex conjugate feedback can exhibit explosive transitions and multistabilities*. Interestingly, we show that the additional complex conjugate feedback induces distinct symmetry-breaking states as well as an explosive transition to an amplitude death state.

In order to find out the effect of an additional complex conjugate feedback factor, we considered a network of globally coupled Stuart-Landau (SL) oscillators. With increasing feedback strength of the additional conjugate coupling, we

find a transition from a complete synchronization (CS) to nontrivial amplitude death (NAD) via symmetry breaking clusters (SBCs) and out-of-phase clusters (OPCs). Remarkably, an explosive transition to amplitude death is observed with the variation of the complex conjugate feedback factor. Interestingly, the hysteresis width decrease with the coupling strength of the global coupling is analyzed using the amplitude order parameter, and we find the existence of a first-order transition with hysteresis. In addition, the global dynamical transitions are illustrated in parametric space to map the occurrence of explosive transitions and multistabilities. Increasing the strength or frequency of feedback enhances the multistability regions. The observed multistability regions are confirmed further by performing a bifurcation analysis and a basin of attraction in the reduced model. Furthermore, the stability condition for NAD is obtained using linear stability (LS) analysis.

The rest of the article is organized as follows: The model of globally coupled SL oscillators is introduced with additional conjugate feedback in Sec. II. Following this, the corresponding dynamical states and their transitions are analyzed in Sec. III; particularly, in Secs. III and IV, we show the existence of explosive transitions and the corresponding dynamical behaviors in the parametric spaces. Further, to confirm the existence of distinct multistability among the dynamical states, we illustrated the one-parameter bifurcation diagram and the basin of attraction using the reduced model in Sec. V. Finally, we summarize our findings in the conclusion, Sec. VI.

II. THE MODEL

To delineate the effect of additional complex conjugate feedback, we consider a general, paradigmatic model of identical Stuart-Landau (SL) oscillators which are coupled through mean-field diffusive coupling [40–44]. Additionally, a complex conjugate mean-field feedback is introduced into the system of globally coupled SL oscillators; the dynamical model reads

$$\dot{w}_k = (\alpha + i\Omega - |w_k|^2)w_k + \varepsilon[\bar{w} - w_k] + \eta[\bar{w}^*], \quad k = 1, 2, \dots, M, \quad (1)$$

where M is the chosen number of oscillators ($M = 100$ in our studies). $w_k = x_k + iy_k$. α is the Hopf bifurcation parameter and Ω is the system frequency. Here $\bar{w} = \frac{1}{M} \sum_{k=1}^M w_k$ is the mean-field and $\bar{w}^* = \frac{1}{M} \sum_{k=1}^M w_k^*$ or $\frac{1}{M} \sum_{k=1}^M (x_k - iy_k)$ is the conjugate mean-field. ε (>0) is the coupling strength of the conventional mean-field diffusive coupling and η (>0) is the strength of the complex conjugate mean-field feedback. The numerical simulations are carried out using fourth-order Runge-Kutta algorithm with a fixed step size $h = 0.01$. In the following, we will mainly explore the effect of the additional feedback factor η on the dynamics of the system.

III. DYNAMICAL STATES AND THEIR TRANSITIONS

In the absence of additional conjugate feedback, i.e., $\eta = 0.0$, the coupled system Eq. (1) exhibits complete synchronization for all the nonzero values of coupling strength ε . When the additional feedback is introduced into the coupled

system, it results in the existence of two different cluster states and nontrivial amplitude death while increasing the feedback strength η . Spatiotemporal evolution and snapshots of the observed dynamical states are demonstrated in Fig. 1 for $\varepsilon = 0.2$ ($\Omega = 1.3$). The inset in each of the snapshots represents the time evolution of representative oscillators x_1 and x_{51} . Figure 1(a) shows the emergence of complete synchronization (CS) for $\eta = 0.2$. Due to the coherent oscillatory behavior of the CS state, all the x_j variables take the same value in the snapshot as depicted in Fig. 1(e). The time series trajectory of the representative oscillators x_1 and x_{51} are also synchronized and oscillates with the same amplitudes and zero phase difference, as can be seen in the inset in Fig. 1(e). If the feedback strength is increased, we find that the oscillators in the network split into two subgroups and result in two cluster states: this is shown in Fig. 1(b) for $\eta = 1.3$. Interestingly, we noticed that the observed x_j variables of the two clusters have asymmetric values, as depicted in Fig. 1(f). Such cluster states is referred to as symmetry breaking clusters (SBCs) [45,46]. From the inset in Fig. 1(f), it is clear that the oscillators x_1 and x_{51} from the two different clusters oscillate with different amplitudes and phases. Further increase in the feedback strength results in symmetric clusters with π phase difference. Therefore, the values are exactly equal and take opposite signs [see Figs. 1(c) and 1(g) for $\eta = 1.5$], and are further referred as out-of-phase clusters (OPCs). The representative oscillators x_1 and x_{51} from the OPC state have identical amplitudes but with a π phase difference [see the inset in Fig. 1(g)]. Further increase in η gives rise to an oscillation quenching state. Here, we observe a nontrivial amplitude death (NAD) state as seen in Figs. 1(d) and 1(h). In NAD, all the oscillators attain the same steady state with nontrivial coupling dependent nonzero value, as is evident from Fig. 1(h) and the representative oscillators in the inset. In the next section, we point out the occurrence of explosive transition as a function of the feedback strength in the following.

IV. EXPLOSIVE TRANSITIONS

To illustrate the occurrence of explosive transition due to additional conjugate feedback, we have plotted the normalized average amplitude order parameter as a function of η as shown in Fig. 2. The order parameter in terms of normalized average amplitude [$R_A(\eta)$] is defined by

$$R_A(\eta) = \frac{A(\eta)}{A(0)}, \quad (2)$$

where $A(\eta)$ is estimated by finding the difference between the global maxima and minima of all the oscillators averaged over a long time interval at a particular feedback strength which can be defined as $A(\eta) = (\sum_{k=1}^M \langle x_{k,\max} \rangle_t - \sum_{k=1}^M \langle x_{k,\min} \rangle_t) / M$. $A(0)$ denotes the average amplitude of the oscillators in the absence of feedback. In the death state, $R_A(\eta)$ takes null value, otherwise $R_A(\eta) > 0$ for the oscillatory state. Primarily, we have plotted the amplitude order parameter for variation in η for a fixed coupling strength $\varepsilon = 0.2$. We can note that on increasing the feedback strength the system exhibits a first-order transition, that is, a transition from higher amplitudes to null value of amplitude at a critical

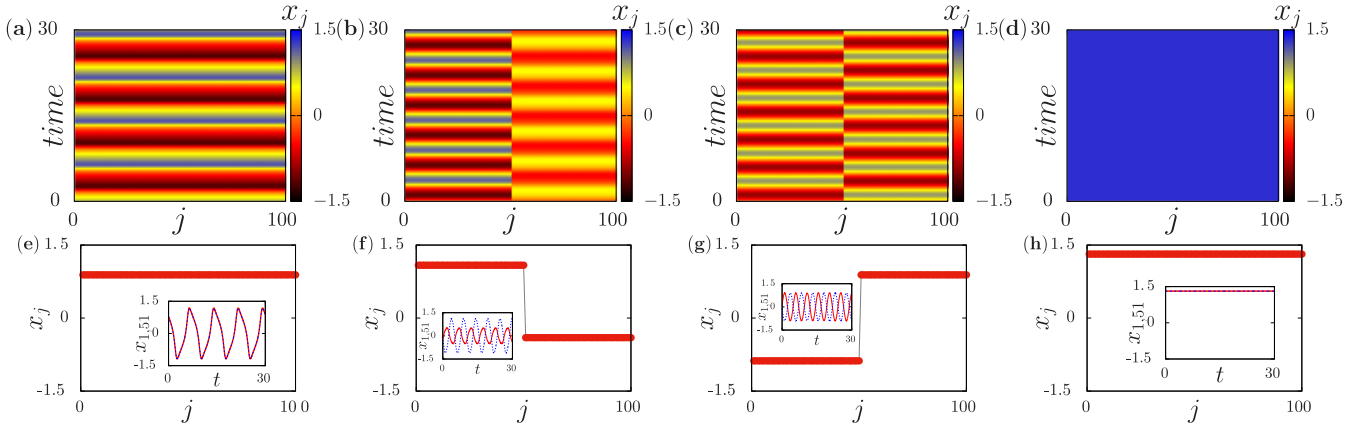


FIG. 1. Spatiotemporal evolution of globally coupled Stuart-Landau oscillators with additional conjugate feedback strengths (a) $\eta = 1.0$ (complete synchronization CS), (b) $\eta = 1.3$ (symmetry breaking clusters SBC), (c) $\eta = 1.5$ (out-of-phase clusters OPC), and (d) $\eta = 2.0$ (nontrivial amplitude death NAD). (e)–(h) are the corresponding snapshots of x_j variables and the insets represent the time evolution of representative oscillators x_1 and x_{51} . Other parameters are $\varepsilon = 0.2$, $\Omega = 1.3$, $\alpha = 1.0$, and $N = 100$.

feedback strength $\eta = 1.6$ during the forward transition, as shown in Fig. 2(a). Interestingly, one notes that the amplitude order parameter takes an intermediate value for the feedback strength in the range $1.3 \leq \eta \leq 1.6$. The reverse transition (i.e., decreasing η) results in a first-order transition from null value amplitude to high values at $\eta = 1.3$. Importantly, in the intermediate region, the SBCs or OPCs coexist with the NAD state. Due to this coexistence, the forward and reverse transitions exhibit a hysteresis behavior. Such first-order transition to death with hysteresis confirms the appearance of explosive death. Furthermore, the amplitude order parameter is plotted for increased values of the coupling strength to $\varepsilon = 0.4$ and $\varepsilon = 0.6$ in Figs. 2(b) and 2(c). We also observe that increasing coupling strength ε reduces the hysteresis area and suppresses it completely at a larger coupling strength.

V. DYNAMICAL TRANSITIONS IN THE PARAMETRIC SPACES

Furthermore, for a more clear understanding of the explosive transitions and multistabilities, we analyze the dynamical behavior of the system specified by Eq. (1) through parametric spaces in detail. Initially, to understand the dynamical transitions in the parametric space, the two-parameter diagrams are plotted in (ε, η) parametric space in Fig. 3 by fixing the frequency at four different values, namely $\Omega = 1.3, 1.5, 2.0$, and $\Omega = 3.0$. The striped patterns indicate the hysteresis area. In Fig. 3(a) for $\Omega = 1.3$, at lower feedback strength with

increasing coupling strength, the system (1) exhibits a complete synchronization behavior for the full range of coupling strength. Increasing the feedback strength, the system (1) gives rise to multistabilities between SBC and NAD as well as OPC and NAD states represented by the regions R_1 and R_2 , respectively. Increasing the feedback to larger values, one finds a suppression of the multistability regions and one finds NAD regions in the entire parametric space. On increasing the frequency to $\Omega = 1.5$, we observe that the CS region is increased. Subsequently, the R_2 region is suppressed with the onset of additional multistability regions R_3 and R_4 . In these regions, CS coexists with OPC and SBC states, respectively. Increasing the frequency further to $\Omega = 1.5$ and $\Omega = 2.0$, one finds the R_3 region gets widened, while the region R_4 is reduced.

In order to illustrate the occurrence of multistabilities and explosive transition due to the additional conjugate feedback, the two-parameter diagrams are also plotted in Fig. 4 by fixing the feedback strength at different values. For feedback strength $\eta = 1.0$, an increasing frequency manifests in a transition from NAD to CS for all values of coupling strength[see Fig. 4(a)]. Interestingly, we noticed the onset of the SBC region at certain critical values of ε and Ω in the NAD region (denoted as R_2). Increasing the feedback strength to $\eta = 1.2$ [depicted in Fig. 4(b)], one finds that the system (1) gives rise to wider region of R_2 . Also, we noticed the existence of the R_1 region at lower frequencies. On increasing the feedback strength to $\eta = 1.5$, one finds that the R_2 region diminishes.

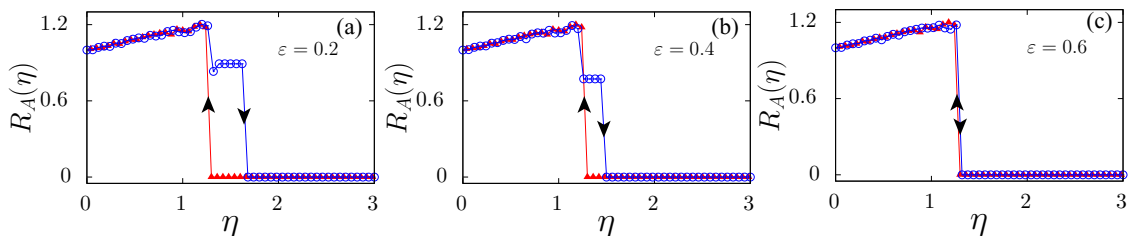


FIG. 2. Amplitude order parameter as a function of η for mean-field coupling strengths (a) $\varepsilon = 0.2$, (b) $\varepsilon = 0.4$, and (c) $\varepsilon = 0.6$. The lines connecting the unfilled circles and the filled triangles denote the forward (down arrow) and backward (up arrow) transitions, respectively.

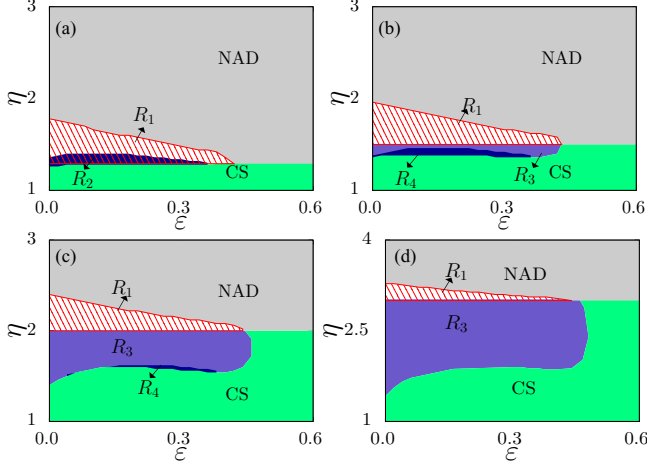


FIG. 3. Two-parameter diagrams in (ϵ, η) space (a) for $\Omega = 1.3$, (b) for $\Omega = 1.5$, (c) for $\Omega = 2.0$, and (d) for $\Omega = 3.0$. CS and NAD are the complete synchronization and nontrivial amplitude death states, respectively. R_1 , R_2 , R_3 , and R_4 are the multistability regions of OPC-NAD, SBC-NAD, OPC-CS, and CS-SBC, respectively.

Eventually, we observe two additional different multistability regions R_3 and R_4 [see Fig. 4(c)]. Upon increasing the feedback as shown in Fig. 4(d), one observes an enlarged R_3 region. From the above observations, it is clear that the additional conjugate feedback results in interesting multistability among the dynamical states in the parametric space.

VI. DYNAMICAL BEHAVIORS THROUGH REDUCED MODEL

In order to understand the genesis of the explosive transition and multistability, we perform a bifurcation analysis and basin stability analysis in the following. For this purpose, we reduce our considered system [Eq. (1)], by splitting the

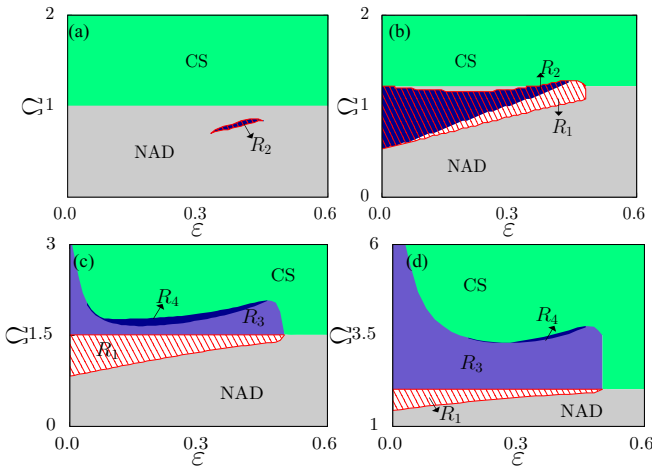


FIG. 4. Two parameter diagram in ϵ, Ω space for (a) $\eta = 1.0$, (b) $\eta = 1.2$, (c) $\eta = 1.5$, and (d) $\eta = 2.0$. CS and NAD are the complete synchronization and nontrivial amplitude death, respectively. R_1 , R_2 , R_3 , and R_4 are the multistability regions of OPC-NAD, SBC-NAD, OPC-CS, and CS-SBC, respectively.

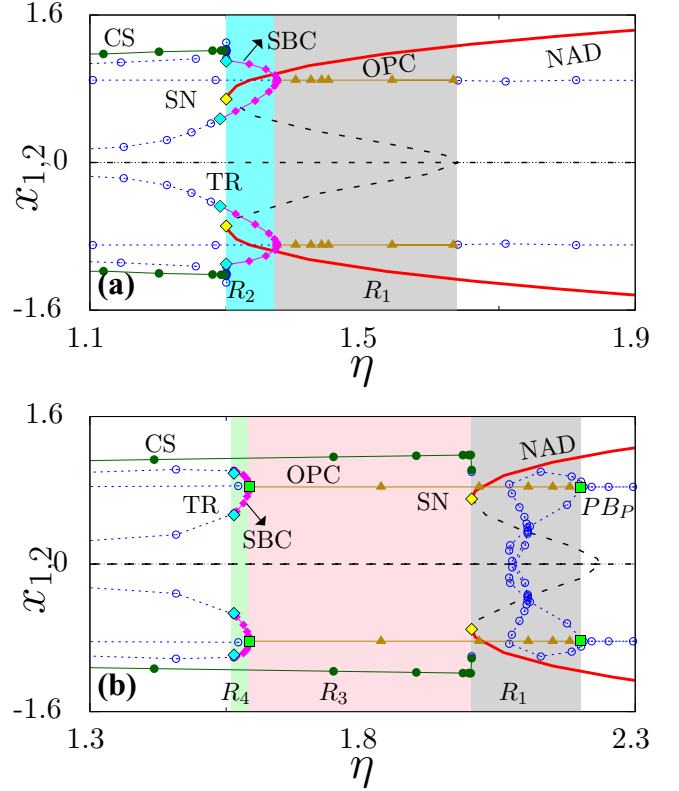


FIG. 5. One-parameter bifurcation diagram for (a) $\epsilon = 0.2$, $\Omega = 1.3$ and (b) $\epsilon = 0.3$, $\Omega = 2.0$. R_1 , R_2 , R_3 , and R_4 are the multistability regions of OPC-NAD, SBC-NAD, OPC-CS, and CS-SBC, respectively. The lines connecting filled circles, diamonds, and triangles denote the stable CS, SBC, and OPC states, respectively. CS, SBC, and OPC are the complete synchronization, symmetry-breaking clusters, and out-of-phase clusters, respectively. NAD represents the nontrivial amplitude death state. TR, SN, and PB_P denote the torus, saddle-node, and pitchfork bifurcation points, respectively. The solid red line represents the stable steady state. The open circles and dashed lines indicate the unstable steady state and unstable oscillations, respectively.

network into two groups $w_k = W_1$ for $k = 1, 2, \dots, M(1 - p)$ and $w_k = W_2$ for $k = M(1 - p) + 1, \dots, M$, where $p = 0.5$. The corresponding dynamical equations can be written as

$$\begin{aligned} \dot{W}_1 &= (\alpha + i\Omega - |W_1|^2)W_1 + \frac{\epsilon}{2}(W_2 - W_1) + \frac{\eta}{2}\overline{W}^*, \\ \dot{W}_2 &= (\alpha + i\Omega - |W_2|^2)W_2 + \frac{\epsilon}{2}(W_1 - W_2) + \frac{\eta}{2}\overline{W}^*, \end{aligned} \quad (3)$$

where $\overline{W}^* = W_1^* + W_2^*$. To show the dynamical transitions and multistability, primarily we have plotted the one-parameter bifurcation diagram (using XPPAUT [47]) by fixing $\epsilon = 0.2$, $\Omega = 1.3$ in Fig. 5(a). Increasing the feedback strength shows a direct transition from a homogeneous oscillatory state to a homogeneous steady state that is CS to NAD through saddle-node bifurcation (SN) at the feedback strength $\eta = 1.3$. In addition for a particular value of feedback ($\eta = 1.29$) the onset of the SBC takes place through torus (TR) bifurcation. The amplitudes of the SBC cluster have

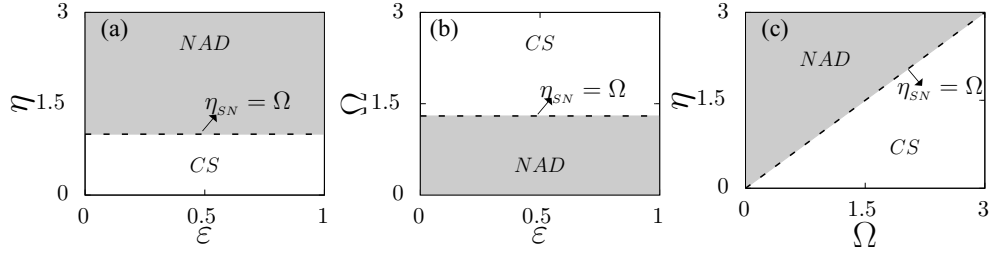


FIG. 6. Stable NAD regions in (a) (ε, Ω) space for $\eta = 1.0$, (b) (ε, η) space for $\Omega = 1.0$, and (c) (Ω, η) space for $\varepsilon = 1.0$. The dashed line in each figure indicates the stability curve which separates CS and NAD states.

different values which decrease while the value of η increases and attains the same values of amplitude where it transits to OPC. Further, the OPC state loses its stability at a critical feedback strength $\eta = 1.7$ and attains the NAD state. The shaded regions represent the multistability regions R_1 and R_2 , respectively.

In addition, to delineate other multistability zones, we set the parameters at $\varepsilon = 0.3$ and $\Omega = 2.0$ and depict a one-parameter diagram, as shown in Fig. 5(b). The bifurcation diagram clearly shows that increasing the value of η results in the birth of SBC through the TR bifurcation, which coexists with CS shown by R_4 . As η increases, the SBC state transits to the OPC state. The CS state coexists with the OPC state in the area of multistability region R_3 . If the feedback is increased further, the coexistence of the OPC and NAD regions (denoted by R_1) is revealed.

Further, one can also determine the stability criterion for the oscillation quenching state using the reduced model. In order to find the stability of the observed nontrivial amplitude death state, we first estimate the fixed point $(x_1, y_1, x_2, y_2) = (\pm x^*, \pm y^*, \pm x^*, \pm y^*)$ using Eq. (3),

$$\begin{aligned} x^* &= \mp \frac{\sqrt{\eta + \alpha - \frac{\Omega^2}{\eta} - \frac{\tilde{\eta}}{\eta^2}}}{\sqrt{2}}, \\ y &= \mp \frac{\eta^3 + \eta^2 \alpha - \tilde{\eta}}{\eta(\eta + \alpha)\Omega} x^*, \end{aligned} \quad (4)$$

where $\tilde{\eta} = \sqrt{\eta^2(\eta + \alpha)^2(\eta^2 - \Omega^2)}$. Further, by finding the Jacobian matrix of Eq. (3) the eigenvalues are obtained, and are expressed as

$$\begin{aligned} \lambda_{1,2} &= \alpha - 2r^* \mp \sqrt{r^{*2} - \Omega^2}, \\ \lambda_{3,4} &= \alpha - 2r^* \mp \sqrt{r^{*2} - 2d^* + \eta^2 - \Omega^2}, \end{aligned} \quad (5)$$

where $r^* = x_1^{*2} + y_1^{*2}$ and $d^* = y_1^{*2} - x_1^{*2}$. The stability condition for NAD is identified by equating the real part of the eigenvalues to zero, and is obtained as $\eta_{SN} = \Omega$.

Using the stability condition $\eta_{SN} = \Omega$, we present the stable NAD region in different parametric spaces in Fig. 6. The stability curve for the NAD region, which separates the CS and NAD regions, is shown by the dashed line in each diagram. From Fig. 6(a), it is clear that for $\eta = 1.0$ the stable boundary exists at $\Omega = 1$ and the stability region occurs for $\Omega \leq 1.0$ for all values of ε . Analogously, from Fig. 6(b) in

(ε, η) space, the stability region occurs at $\eta = 1$ and $\eta \geq 1.0$ for all values of ε and $\Omega = 1$. Furthermore, for any value of ε , the stable NAD region in (Ω, η) space exists when $\eta_{SN} \geq \Omega$, as seen in Fig. 6(c). It is also noticed that the fixed points and stability conditions of NAD are independent of the coupling strength (ε). Hence, the boundary does not change with respect to ε . It can be seen that the stable boundaries of NAD region match well with the numerically obtained NAD region [cf. Figs. 4(a) and 3(a)].

To validate the existence of bistability among the dynamical states, the basin of attraction is plotted in Fig. 7 using Eq. (2) by fixing the initial state of $y_1(0)$ and $y_2(0)$ and by varying $x_1(0)$ and $x_2(0)$ [48]. First, the upper panel A is plotted by fixing $\varepsilon = 0.2$ and $\Omega = 1.3$ for different values of feedback strength. For $\eta = 1.1$, we can observe that the entire initial state space is filled with a complete synchronization state as shown in Fig. 7(a)(i). If the feedback strength is increased to $\eta = 1.37$, we notice that some of the asymmetric initial states favor SBC and the remaining initial states favor the NAD state [see Fig. 7(a)(ii)]. Here, the asymmetric initial states represented by $x_1(0)$ reach positive initial states while $x_2(0)$ attains negative values or vice versa. Thus, Fig. 7(a)(ii) provides evidence for the coexistence of SBC and NAD. Further, on increasing the feedback strength to $\eta = 1.5$, one observes that SBC gets wiped out by OPC [see Fig. 7(a)(iii)]. Upon increasing the feedback strength further we find that the entire initial state space is occupied by the NAD state [see Fig. 7(a)(iv)]. Similarly, panel B is plotted for $\varepsilon = 0.3$, $\Omega = 2.0$, which corresponds to Fig. 5(b). For $\eta = 1.3$, we observed that the entire basin is filled with the CS state, as shown in Fig. 7(b)(i). When the feedback strength is increased to $\eta = 1.58$, certain asymmetric initial states result in the SBC state, while the others lead to the CS state [see Fig. 7(b)(ii)]. If the feedback is increased to $\eta = 1.8$, the SBC transits to the OPC state, which coexists with the CS state, as shown in Fig. 7(b)(iii). When the feedback strength is increased further ($\eta = 2.0$), the CS in the basin is completely suppressed. Finally, the NAD state occupies the basin instead of the CS state [see Fig. 7(b)(iv)]. As the feedback gets stronger, it acquires NAD for the entire basin, as shown in Fig. 7(b)(v). From these observations, it is clear that the onset of multistability among the dynamical states is the major impact of feedback strength.

VII. CONCLUSIONS

The feedback factor is known to be vital for reviving oscillation death or restoring rhythmicity in a dynamical system.

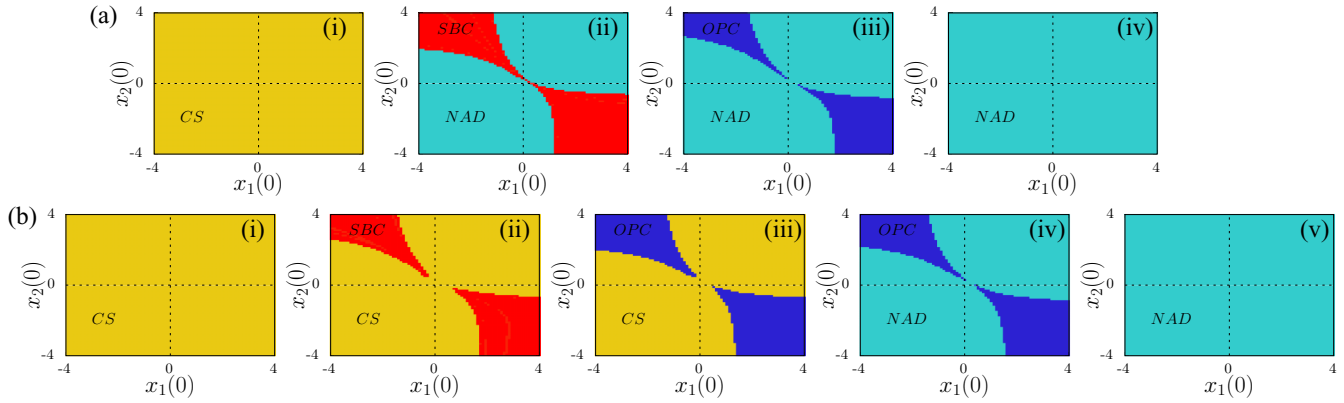


FIG. 7. Basin of attraction by fixing the initial states at $y_1(0) = 0.5$ and $y_2(0) = 0.45$ and varying $x_1(0)$ and $x_2(0)$ for panel (a): (i) $\eta = 1.1$, (ii) $\eta = 1.37$, (iii) $\eta = 1.5$, and (iv) $\eta = 1.8$. For panel (b): (i) $\eta = 1.3$, (ii) $\eta = 1.58$, (iii) $\eta = 1.8$, (iv) $\eta = 2.0$, and (v) $\eta = 2.3$. The other parameters for the panels (a) and (b) are fixed corresponding to Figs. 5(a) and 5(b), respectively.

The purpose of this study is to analyze whether the feedback component may lead to explosive death and multistability. To accomplish this, we have considered a system of globally coupled Stuart-Landau oscillators with conjugate feedback. We first looked at dynamical transitions by increasing the feedback factor. We discovered that the transition from complete synchronization (CS) to nontrivial amplitude death (NAD) occurs via symmetry breaking clusters (SBCs) and out-of-phase clusters (OPCs). The emergence of explosive transitions is demonstrated using the amplitude order parameter as a function of feedback strength. The occurrence of first-order transitions is linked to hysteresis behavior.

The region of multistable states is found to be governed by the interplay of feedback factors and the natural frequency of the coupled oscillators. For a better understanding of the observed scenarios, we have considered a reduced model and carried out a detailed bifurcation analysis and a linear stability analysis, which are in good accord with the numerical results of the extended system. The obtained results imply that the globally coupled oscillators exhibit an explosive death and distinct multistable states as a result of additional conjugate

feedback. Additionally, the proposed work raises many open problems. For instance, extending our study to different topological structures, such as scale free, small world, and others, is a practical realization. Feedback is a common way to restore dynamism to the degraded dynamical units in a complex network, and it is also crucial to investigate the effects of different feedbacks.

Our findings may offer insight into the impact of additional feedback in many biological systems where feedback appears naturally to regulate physiological mechanisms [49,50] and in engineering systems where often feedback is intentionally introduced for control purposes (e.g., in phase-locked loops and laser systems [51,52]).

ACKNOWLEDGMENTS

The work of D.P. is funded by the Center for Nonlinear Systems, Chennai Institute of Technology, India, via funding number CIT/CNS/2022/RP-016. M.L. is supported by a DST-SERB National Science Chair position (Ref. No. NSC/2020/000029).

-
- [1] S. Herzog, C. Tetzlaff, and F. Wörgötter, *Neural Networks* **123**, 153 (2020).
 - [2] S. C. Kak, *Circuits Syst. Signal Process.* **12**, 263 (1993).
 - [3] S. Draghici, *Int. J. Neural Syst.* **08**, 113 (1997).
 - [4] M. C. D. Bock, R. Denk, C. T. Wirth, P. Goldberg-Oppenheimer, S. Hofmann, and J. J. Baumberg, *Appl. Phys. Lett.* **100**, 013112 (2012).
 - [5] F. Nazarimehr, K. Rajagopal, J. Kengne, S. Jafari, and V. T. Pham, *Chaos Solitons Fractals* **111**, 108 (2018).
 - [6] K. Rajagopal, A. Bayani, A. J. M. Khalaf, H. Namazi, S. Jafari, and V. T. Pham, *AEU Int. J. Electron. Commun.* **95**, 207 (2018).
 - [7] K. Rajagopal, A. Akgul, S. Jafari, and B. Aricioglu, *Nonlinear Dyn.* **91**, 957 (2018).
 - [8] K. Rajagopal, S. Jafari, A. Karthikeyan, A. Srinivasan, and B. Ayele, *Circuits Syst. Signal Process.* **37**, 3702 (2018).
 - [9] V. Sundarapandian and R. Karthikeyan, *Internatl. J. Soft Comput.* **6**, 111 (2011).
 - [10] A. Ozawa and H. Kori, *Phys. Rev. E* **103**, 062217 (2021).
 - [11] V. K. Chandrasekar, S. Karthiga, and M. Lakshmanan, *Phys. Rev. E* **92**, 012903 (2015).
 - [12] W. Zou, V. K. Senthilkumar, R. Nagao, I. Z. Kiss, Y. Tang, A. Koseska, J. Duan, and J. Kurths, *Nat. Commun.* **6**, 1 (2015).
 - [13] D. Ghosh, T. Banerjee, and J. Kurths, *Phys. Rev. E* **92**, 052908 (2015).
 - [14] J. Palanivel, K. Suresh, D. Premraj, and K. Thamilmaran, *Chaos Solitons Fractals* **106**, 35 (2018).
 - [15] D. Premraj, K. Suresh, T. Banerjee, and K. Thamilmaran, *Chaos* **27**, 013104 (2017).
 - [16] D. Premraj, K. Suresh, T. Banerjee, and K. Thamilmaran, *Phys. Rev. E* **98**, 022206 (2018).
 - [17] T. Banerjee and D. Biswas, *Chaos* **23**, 043101 (2013).

- [18] T. Banerjee and D. Ghosh, *Phys. Rev. E* **89**, 052912 (2014).
- [19] T. Banerjee, *Europhys. Lett.* **110**, 60003 (2015).
- [20] T. Banerjee, D. Biswas, D. Ghosh, B. Bandyopadhyay, and J. Kurths, *Phys. Rev. E* **97**, 042218 (2018).
- [21] K. Ponrasu, U. Singh, K. Sathiyadevi, D. V. Senthilkumar, and V. K. Chandrasekar, *Chaos* **30**, 053120 (2020).
- [22] U. Singh, K. Sathiyadevi, V. K. Chandrasekar, W. Zou, J. Kurths, and D. V. Senthilkumar, *New J. Phys.* **22**, 093024 (2020).
- [23] D. Biswas, T. Banerjee, and J. Kurths, *Phys. Rev. E* **94**, 042226 (2016).
- [24] D. Biswas, T. Banerjee, and J. Kurths, *Chaos* **27**, 063110 (2017).
- [25] K. Ponrasu, K. Sathiyadevi, V. K. Chandrasekar, and M. Lakshmanan, *Europhys. Lett.* **124**, 20007 (2018).
- [26] K. Sathiyadevi, I. Gowthaman, D. V. Senthilkumar, and V. K. Chandrasekar, *Chaos* **29**, 123117 (2019).
- [27] I. Gowthaman, K. Sathiyadevi, V. K. Chandrasekar, and D. V. Senthilkumar, *Nonlinear Dyn.* **101**, 53 (2020).
- [28] K. Sathiyadevi, D. Premraj, T. Banerjee, Z. Zheng, and M. Lakshmanan, *Chaos Solitons Fractals* **157**, 111944 (2022).
- [29] S. Kundu, S. Majhi, and D. Ghosh, *Phys. Rev. E* **97**, 052313 (2018).
- [30] A. D. Kachhvah and S. Jalan, *Phys. Rev. E* **104**, L042301 (2021).
- [31] A. Kumar, S. Jalan, and A. D. Kachhvah, *Phys. Rev. Res.* **2**, 023259 (2020).
- [32] N. Bastas, P. Giazitidis, M. Maragakis, and K. Kosmidis, *Physica A* **407**, 54 (2014).
- [33] S. Fortunato and H. Satz, *Nucl. Phys. B Proc. Suppl.* **106-107**, 890 (2002).
- [34] H. Bi, X. Hu, X. Zhang, Y. Zou, Z. Liu, and S. Guan, *Europhys. Lett.* **108**, 50003 (2014).
- [35] U. K. Verma, A. Sharma, N. K. Kamal, J. Kurths, and M. D. Shrimali, *Sci. Rep.* **7**, 1 (2017).
- [36] U. K. Verma, A. Sharma, N. K. Kamal, and M. D. Shrimali, *Phys. Lett. A* **382**, 2122 (2018).
- [37] N. Zhao, Z. Sun, X. Yang, and W. Xu, *Phys. Rev. E* **97**, 062203 (2018).
- [38] Z. Sun, S. Liu, and N. Zhao, *Chaos Solitons Fractals* **142**, 110514 (2021).
- [39] S. Dixit, S. N. Chowdhury, D. Ghosh, and M. D. Shrimali, *Europhys. Lett.* **133**, 40003 (2021).
- [40] D. G. Aronson, G. B. Ermentrout, and N. Kopell, *Physica D* **41**, 403 (1990).
- [41] G. B. Ermentrout, *Physica D* **41**, 219 (1990).
- [42] E. Panteley, A. Loria, and A. El Ati, *IFAC-PapersOnLine* **48**, 645 (2015).
- [43] D. Premraj, K. Manoj, S. A. Pawar, and R. I. Sujith, *Nonlinear Dyn.* **103**, 1439 (2021).
- [44] L. Tumash, E. Panteley, A. Zakharova, and E. Schöll, *Eur. Phys. J. B* **92**, 1 (2019).
- [45] K. Sathiyadevi, V. K. Chandrasekar, and M. Lakshmanan, *Phys. Rev. E* **105**, 034211 (2022).
- [46] K. Sathiyadevi, V. K. Chandrasekar, and D. V. Senthilkumar, *Nonlinear Dyn.* **98**, 327 (2019).
- [47] B. Ermentrout, *Simulating, Analyzing, and Animating Dynamical Systems: A Guide to XPPAUT for Researchers and Students (Software, Environments, Tools)* (SIAM, Philadelphia, 2002).
- [48] I. Śliwa, and K. Grygiel, *Nonlinear Dyn.* **67**, 755 (2012).
- [49] M. E. Kotas and R. Medzhitov, *Cell* **160**, 816 (2015).
- [50] S. I. Park, C. Lee, W. D. Sadler, A. J. Koh, J. Jones, J. W. Seo, F. N. Soki, S. W. Cho, S. D. Daignault, and L. K. McCauley, *Cancer Res.* **73**, 6574 (2013).
- [51] T. Banerjee and B. C. Sarkar, *Int. J. Electron.* **96**, 717 (2009).
- [52] E. Schöll, and H. G. Schuster, *Handbook of Chaos Control*, 2nd ed. (Wiley-VCH, Weinheim, 2007).